

# Sensorless Vibration Suppression and Scan Compensation for Piezoelectric Tube Nanopositioners

Andrew J. Fleming, *Member, IEEE* and S. O. Reza Moheimani, *Senior Member, IEEE*

**Abstract**—Piezoelectric tube scanners are employed in high-resolution positioning applications such as scanning probe microscopy and nanofabrication. Much research has proceeded with the aim of reducing hysteresis and vibration—the two foremost problems associated with piezoelectric tube scanners. In this paper, two simple techniques are proposed for simultaneously reducing hysteresis and vibration: 1) A new dc accurate charge amplifier is shown to significantly reduce hysteresis while avoiding characteristic voltage drift. 2) Piezoelectric shunt damping, a technique previously resident in the field of smart structures, has been applied to damp tube vibration. By attaching an LCR impedance to a single tube electrode, the first mechanical mode is reduced in magnitude by more than 20 dB.

**Index Terms**—Charge control, hysteresis, nanopositioning, piezoelectric tube, scanning probe microscope, scan compensation, shunt damping.

## I. INTRODUCTION

PIEZOELECTRIC tube scanners were first reported in [1] for use in scanning tunneling microscopes [2]. They were found to provide a higher positioning resolution and greater bandwidth than traditional tripod positioners whilst being simple to manufacture and easier to integrate into a microscope. Piezoelectric tube scanners are now used extensively in scanning probe microscopes and many other applications requiring precision positioning, e.g., nanomachining [3], [4], etc.

As shown in Fig. 1(a), a piezoelectric scanner comprises a tube of radially poled piezoelectric material, four external electrodes, and a grounded internal electrode. Other configurations may include: a circumferential electrode for independent vertical extension or diameter contraction, and/or sectorized internal electrodes. Small-deflection expressions for the lateral tip translation, derived from the IEEE Piezoelectricity Standard [5], can be found in [6]. Measured in the same axis ( $x$  or  $y$ ) as the applied voltage, the tip translation  $d$  is approximately

$$d_i = \frac{\sqrt{2}d_{31}L^2}{\pi Dh}v_i \quad i = x, y \quad (1)$$

where  $d_i$  is the ( $x$  or  $y$  axis) deflection,  $d_{31}$  is the piezoelectric strain constant,  $L$  is the length of the tube,  $D$  is the outside diameter,  $h$  is the tube thickness, and  $v_i$  is the ( $x$  or  $y$  axis) electrode voltage. Tip deflection can be doubled by applying

an equal and opposite voltage to electrodes in the same axis. Vertical translation due to a voltage applied equally to all four quadrants is given approximately by

$$\Delta L = \frac{2d_{31}L}{h}v. \quad (2)$$

Although the statics and dynamics of piezoelectric tubes are inherently nonlinear and three-dimensional, tube geometries with large length/diameter ratios can be highly simplified. For such geometries, and in case of small deflection, the tube top can be assumed flat with no vertical excursion or tilting due to lateral deflection. Although there has been some recent effort to consider the coupling from lateral to vertical dimensions, tubes are generally designed to minimize such effects. Other design considerations are the deflection sensitivity and maximum deflection; both of these characteristics are optimized by large length to diameter ratios.

A consequence of designing tubes with large length/diameter ratios is low mechanical resonance frequency. This has been a fundamental problem since the inception of piezoelectric tube scanners. A lightly damped low-frequency mechanical resonance severely limits the maximum achievable scan frequency. A triangular scan rate of around 1/100th the first mechanical resonance frequency is usually assumed the upper limit in precision scanning applications.

Nonlinearity is another on-going difficulty associated with piezoelectric tube scanners (and piezoelectric actuators in general). When employed in an actuating role, piezoelectric transducers display a significant hysteresis in the transfer function from an applied voltage to strain or displacement [7]. Due to hysteresis, ideal scanning signals can result in severely distorted tip displacements, and hence, poor image quality or nanofabrication defects.

Techniques aimed at addressing both mechanical dynamics and hysteresis can be grouped generally into two broad categories, feedforward and feedback. Feedforward techniques, as shown in Fig. 1, do not include a sensor but require accurate knowledge of the undesirable dynamics. Feedback systems, although more robust to modeling error, are limited by the noise performance and bandwidth of the sensor. In many cases it is also difficult and/or prohibitively expensive to integrate displacement sensors into the scanning apparatus.

Feedforward and signal compensation approaches have been extensively studied as their implementation requires no additional hardware or sensors. It should be considered, however, that additional hardware such as displacement sensors and DSP processors are required to identify the behavior of each tube prior to implementation. A technique for designing optimal

Manuscript received December 3, 2004; revised July 11, 2005. Manuscript received in final form August 10, 2005. Recommended by Associate Editor S. Devasia. This work was supported by the Australian Research Council.

The authors are with the School of Electrical Engineering and Computer Science, The University of Newcastle, Australia (e-mail: andrew.fleming@newcastle.edu.au).

Digital Object Identifier 10.1109/TCST.2005.860511

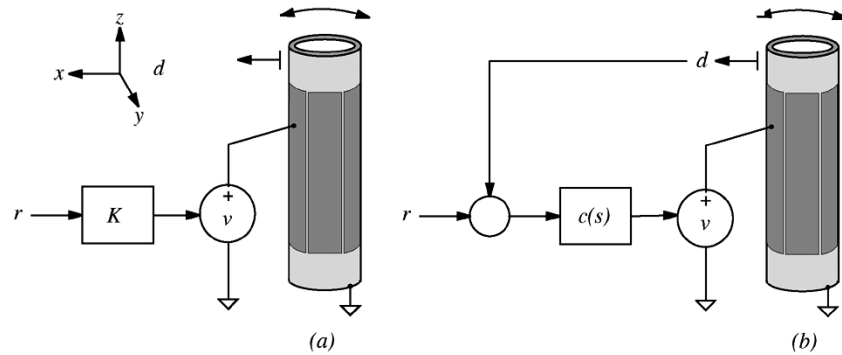


Fig. 1. Voltage driven tube scanner. (a) Open-loop with signal precompensation. (b) Closed-loop with displacement feedback.

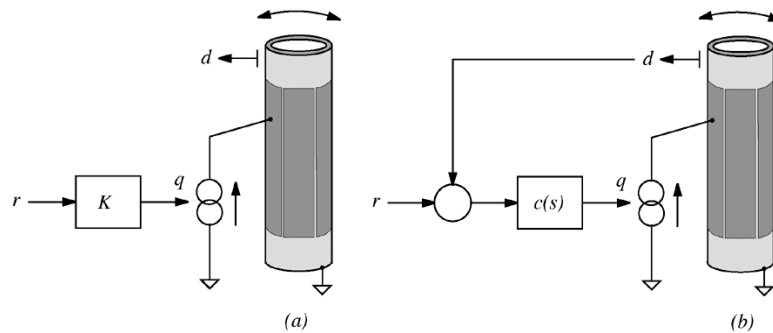


Fig. 2. Charge driven tube scanner. (a) Open-loop with signal precompensation. (b) Closed-loop with displacement feedback.

linear feedforward compensators was presented in [8], then later extended to incorporate a PD feedback controller [3]. In these works, the authors identify the main limitation to performance as being modeling error. Another feedforward technique, known as iterative or learning control is aimed at reducing unmodeled hysteresis. The need for a model is essentially annulled with the use of a sensor and online iteration to ascertain the optimal input compensation [9]. The foremost problems with iterative techniques are the time taken to iterate the compensator and difficulties associated with nonmonotonic trajectories. Other feedforward approaches have included: Optimal  $\mathcal{H}_\infty$  compensation [10]; Compensation for creep, Preisach hysteresis, and resonance [11]; Improved iterative Preisach inversion [12]; and various optimal linear feedforward compensation techniques [13], [14].

Feedback techniques can provide excellent low-frequency tracking performance, but depend heavily on the sensor noise performance and bandwidth. As a consequence, such techniques are most applicable to scan ranges in the hundreds of nanometers or greater. Good tracking of a 5-Hz triangle wave, while maintaining robustness to nonlinearity was presented in [15]. With the integration of displacement sensors into the next generation of commercial microscopes, feedback systems will become more feasible.

Considering the breadth of research aimed at improving scan performance, it is surprising to find that commercial microscope manufacturers have been reluctant to adopt the techniques discussed. The majority of commercial scanning systems operate in much the same fashion as they did in the early 1990s. Regardless of the potential benefits, the requirement for data acquisition, sophisticated modeling experiments, and additional sen-

sors have severely limited the application of feedforward and feedback scan compensation. With this in mind, the research in this paper introduces two simple, nonmodel-based techniques for the reduction of hysteresis and vibration.

Since the late 1980s, it has been known that driving piezoelectric transducers with current or charge rather than voltage significantly reduces hysteresis [16]. Simply by regulating the current or charge, a fivefold reduction in the hysteresis can be achieved [17]. A quote from a recent paper [18] typifies the sentiment toward this technique: “While hysteresis in a piezoelectric actuator is reduced if the charge is regulated instead of the voltage [16], the implementation complexity of this technique prevents a wide acceptance [19].”

Although the circuit topology of a charge or current amplifier is much the same as a simple voltage feedback amplifier, the uncontrolled nature of the output voltage typically results in the load capacitor being charged up. Saturation and distortion occur when the output voltage, referred to as the compliance voltage, reaches the power supply rails. The stated *complexity* invariably refers to the need for additional circuitry to avoid charging of capacitive loads.

The first contribution of this paper is to present a new class of grounded-load charge amplifier free from dc and low-frequency voltage drift. As shown in Fig. 2, voltage amplifiers used in previous techniques can be replaced with a charge amplifier, significant reduction of hysteresis can be achieved. To simplify the adaptation of previous drive techniques, an analysis of the relationship between charge and voltage actuation is provided. In most cases, a constant gain will equate the displacement response of a tube driven by either charge or voltage.

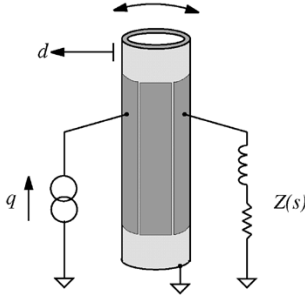


Fig. 3. Charge driven tube scanner with piezoelectric shunt damping circuit.

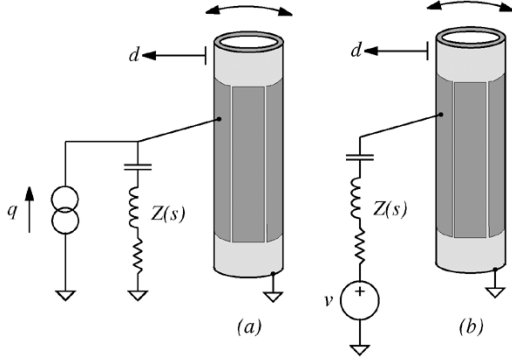


Fig. 4. (a) Charge driven tube scanner. (b) Voltage equivalent circuit.

The second contribution is a new technique for the reduction of scan induced and exogenous vibration. Drawn from the field of Smart Structures, we propose the connection of an electrical impedance to the terminals of one  $x$  and  $y$  electrode. Usually referred to as piezoelectric shunt damping, this technique results in a damped electrical resonance capable of significantly reducing the magnitude of one or more structural modes. Fig. 3 illustrates an inductor and resistor connected to the terminals of a charge driven piezoelectric tube. In this configuration, the inductor and resistor are tuned to damp the first  $x$  axis cantilever mode. Undesired resonance excitation due to scanning and external disturbance is attenuated.

Piezoelectric shunt damping requires no feedback sensor and is thus immune to the usual problems of low-bandwidth and measurement noise associated with optical and capacitive sensors. Furthermore, as illustrated in Fig. 4, we demonstrate that the shunt impedance  $Z(s)$ , can be applied to the same electrode as the driving charge or voltage source. This allows the redundant electrode to be used for increasing the scan range or as a piezoelectric strain sensor. Like the charge amplifier, such a technique can be implemented independently or in conjunction with a previous technique to improve performance.

In Section II, we discuss the modeling of a piezoelectric tube and analyze the effect of a connected shunt impedance. Implementation issues are then discussed in Section III, followed by experimental results and conclusions in Sections IV and V.

## II. SHUNT CIRCUIT MODELING

Modeling of piezoelectric transducers with attached resonant shunt circuits has traditionally been performed using voltage driven models. In this work, only charge driven models are utilized. The following sub-section introduces the models required

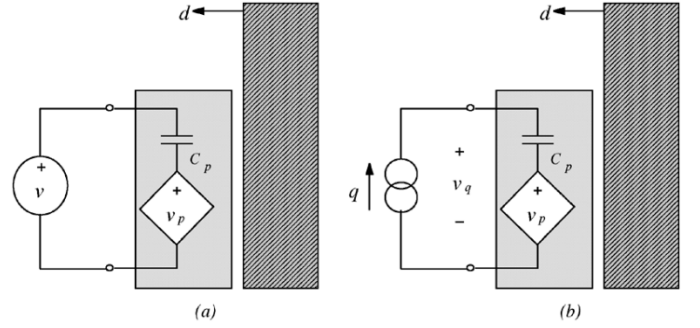


Fig. 5. (a) A voltage and (b) charge driven piezoelectric tube.

to simulate the effect of an attached shunt circuit. Traditional voltage driven models are initially discussed then related to their charge driven equivalents as used throughout.

### A. Open-Loop

We first consider the open-loop translational dynamics of a piezoelectric tube. The electrically equivalent model of a voltage and charge driven piezoelectric tube is shown in Fig. 5. Each electrode acts as a piezoelectric transducer, represented by a strain dependent voltage source  $v_p$  and series capacitor  $C_p$ . The polarization vector is assumed to be oriented radially outward, in this case, a positive voltage or charge results in a positive deflection. We are interested in the transfer functions from an applied voltage  $v$  to the resulting piezoelectric voltage  $v_p$  and tip translation  $d$ , that is

$$G_{vv}(s) = \frac{v_p(s)}{v(s)} \quad G_{dv}(s) = \frac{d(s)}{v(s)}. \quad (3)$$

The transfer functions  $G_{vv}(s)$  and  $G_{dv}(s)$  can be derived analytically or determined experimentally. Due to the difficulties involved with modeling complicated geometries from first principles, empirical models obtained through system identification are preferable.

In the case of charge actuation, Fig. 5(b), equivalent transfer functions can be derived. Kirchoff's Voltage Law for the loop is

$$\frac{-q}{C_p} - v_p + v_q = 0. \quad (4)$$

Substituting  $v_p = G_{vv}v_q$  and simplifying yields

$$G_{vq}(s) = \frac{v_p(s)}{q(s)} = \frac{1}{C_p} \frac{G_{vv}(s)}{1 - G_{vv}(s)}. \quad (5)$$

The displacement transfer function can be derived in a similar fashion

$$G_{dq}(s) = \frac{d(s)}{q(s)} = \frac{1}{C_p} \frac{G_{dv}(s)}{1 - G_{vv}(s)}. \quad (6)$$

Off resonance, where  $G_{vv}(s) \ll 1$

$$G_{vq}(s) \approx \frac{G_{vv}(s)}{C_p} \quad G_{dq}(s) \approx \frac{G_{dv}(s)}{C_p}. \quad (7)$$

Thus, the relationship between charge and voltage actuation is revealed. Due to the benefits in reducing hysteresis, only charge actuation will be considered in the proceeding sections.

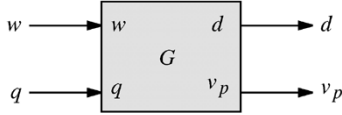


Fig. 6. The piezoelectric tube model describing the deflection  $d$  and strain voltage  $v_p$  in response to an applied charge  $q$  and disturbance  $w$ .

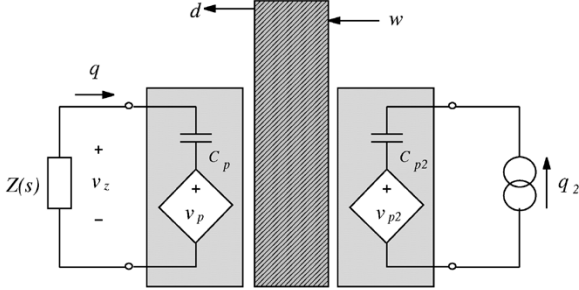


Fig. 7. The electrical equivalent of a charge driven piezoelectric tube with attached shunt circuit.

In addition to a charge input, the possibility for a disturbance input  $w$  is also desirable. The signal  $w$  can be used to study the regulation or rejection of environmental noise. In the following sections the tube system will be referred to as  $G$ , a multi-input multi-output system describing the deflection  $d$  and piezoelectric voltage  $v_p$  in response to a driving charge  $q$  and disturbance  $w$ . The transfer functions  $G_{vq}(s)$  and  $G_{dq}(s)$  are contained in  $G$ . Such a realization is advantageous as the system  $G$  will later be identified directly from experimental data using system identification. The tube model  $G$  is shown in Fig. 6.

### B. Shunt Damping

Although first appearing in [20], the concept of piezoelectric shunt damping is mainly attributed to Hagood and von Flotow [21]. A series inductor-resistor network, as shown in Fig. 3, was demonstrated to significantly reduce the magnitude of a single structural mode. Together with the inherent piezoelectric capacitance, the network is tuned to the resonance frequency of a single structural mode. Analogous to a tuned mechanical absorber, additional dynamics introduced by the shunt circuit act to increase the effective structural damping [21].

The equivalent electrical model of a shunted piezoelectric tube (as shown in Fig. 3) is illustrated in Fig. 7. To find the transfer function relating displacement  $d$  to the driving charge  $q_2$  we start by writing Kirchoff's Voltage Law around the impedance loop and substituting  $v_z = -qsZ(s)$

$$\frac{-q(s)}{C_p} - v_p(s) + -q(s)sZ(s) = 0. \quad (8)$$

When the opposing tube electrodes are equal in dimension, the charges  $q$  and  $q_2$  have an equal but opposite influence on the tube deflection  $d$  and  $v_p$ . Furthermore

$$v_p = -v_{p2} \quad (9)$$

$$\frac{v_p(s)}{q(s)} = \frac{v_{p2}(s)}{q_2(s)} = \frac{-v_p(s)}{q_2(s)} = G_{vq}(s). \quad (10)$$

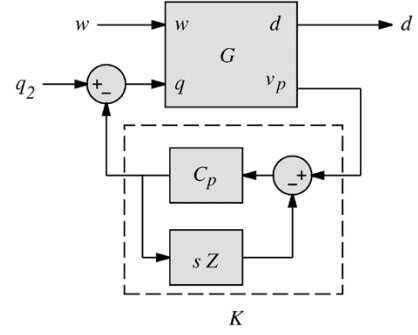


Fig. 8. The equivalent feedback diagram where an electrical impedance is connected to the terminals of one tube electrode and the other is driven with charge.

The principle of superposition can be applied to find an expression for  $v_p$

$$v_p(s) = G_{vq}(s)q(s) - G_{vq}(s)q_2(s). \quad (11)$$

Rearranging (11) in terms of  $q_2$  and substituting into (8) yields

$$\frac{v_p(s)}{q_2(s)} = \frac{-G_{vq}(s)}{1 + G_{vq}(s)K(s)} \quad (12)$$

where

$$K(s) = \frac{C_p}{1 + C_p sZ(s)}. \quad (13)$$

The shunted displacement transfer function can be derived in a similar manner

$$\frac{d(s)}{q_2(s)} = \frac{G_{dq}(s)}{1 + G_{vq}(s)K(s)}. \quad (14)$$

Using the principle of superposition, the influence of an external disturbance  $w$  can also be included

$$d(s) = \frac{1}{1 + G_{vq}(s)K(s)} (G_{dq}(s)q_2(s) + G_{dw}(s)w(s)) \quad (15)$$

where  $G_{dw}$  is the transfer function measured from an external force  $w$  to the displacement  $d$ .

From (14) and (15) it is concluded that the presence of an electrical shunt impedance can be viewed equivalently as a strain-voltage feedback control system. A diagrammatic representation of (15) is shown in Fig. 8. Further interpretation and analysis can be found in [22].

In some cases (where a second electrode is not available), it may be difficult to obtain a model describing the piezoelectric voltage  $v_p$  directly. In such cases, the terminal voltage  $v_z$  can also be considered. The equivalent terminal-voltage feedback diagram is shown in Fig. 9.  $v_z$  is related to  $v_p$  by

$$v_z = v_p + \frac{1}{C_p}q, \quad (16)$$

that is,

$$\frac{v_z(s)}{q(s)} = G_{vq}(s) + \frac{1}{C_p}. \quad (17)$$

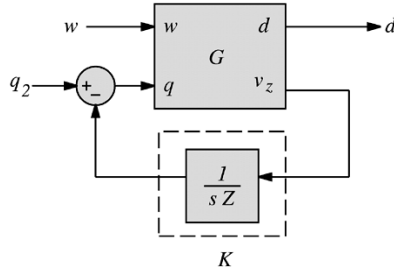


Fig. 9. An alternative feedback interpretation considering the terminal voltage  $v_z$  rather than the piezoelectric voltage  $v_p$ .

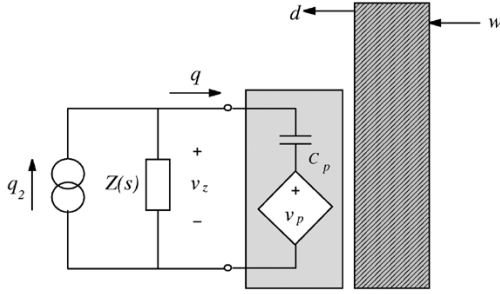


Fig. 10. A charge driven tube electrode with attached parallel shunt circuit.

Equations (8) to (15) can be modified accordingly.

1) *Hybrid Operation:* As mentioned in the introduction, it is advantageous to connect the shunt impedance and driving charge source to the same electrode. This scenario is depicted in Fig. 10. In this subsection, the electrical filtering effect of  $Z(s)$  on  $q_2$  is derived. If such a filtering effect can be inverted, the charge source  $q_2$  can be used for scanning, analogous to the case where a shunt impedance is attached to an independent electrode.

Writing Kirchoffs Voltage Law around the loop

$$-\frac{q}{C_p} - v_p + v_z = 0 \quad (18)$$

and substituting the following

$$q(s) = -\frac{v_z(s)}{sZ(s)} + q_2(s) \quad (19)$$

results in the loop equation

$$-\frac{q(s)}{C_p} - v_p(s) + q(s)sZ(s) + q_2(s)sZ(s) = 0. \quad (20)$$

Given that  $v_p = G_{vq}q$ , we can substitute  $q = v_p/G_{vq}$  into (20). After simplification, the transfer function from  $q_2$  to  $v_p$  can be found

$$\frac{v_p(s)}{q_2(s)} = \frac{K(s)Z(s)G_{vq}(s)}{1 + G_{vq}(s)K(s)}$$

where  $K$  is as given in (13). Similarly,

$$\frac{d(s)}{q_2(s)} = \frac{K(s)Z(s)G_{dq}(s)}{1 + G_{vq}(s)K(s)}. \quad (21)$$

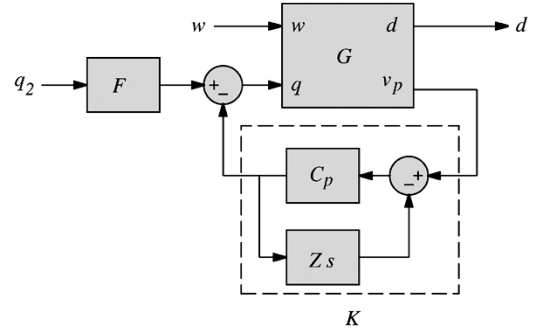


Fig. 11. The equivalent feedback diagram where the driving charge and shunt impedance are applied to the same electrode (as shown in Fig. 10).

Unlike the case in Section II.B, the impedance  $Z(s)$  distorts the tube transfer function from the driving charge  $q_2$  to the deflection  $d$ . Rather than simply adding a strain feedback controller to the mechanical system, the transfer function from  $q_2$  to  $d$  now also contains a filter  $F(s) = K(s)Z(s)$ . An equivalent feedback diagram is shown in Fig. 11.

An obvious technique for recovering the natural tube dynamics is to pre-filter the driving charge with  $F^{-1}(s)$ . Fortunately this prefiltering and inversion is straight-forward to implement in practice. This solution is discussed in Section III.

2) *Shunt Impedance Design:* The Smart Structures and Vibration Control literature contain a multitude of passive, active, linear, and nonlinear piezoelectric shunt impedance designs (reviewed in [23] and [24]). However, only a small subset is suitable for piezoelectric tube damping. The so-called resonant linear shunts meet all of the requisite criteria: They are easy to design, implement, and tune; they offer excellent damping performance (especially for single modes of vibration); they are strictly passive and inject no harmonics; and finally, their presence influences the mechanical dynamics only over a small frequency range. Resonant linear shunts have been shown to emulate the effect of a tuned-mass mechanical absorber [21].

After examination of various impedance designs, the LCR circuit depicted in Fig. 4 was found to offer good performance. The presence of a series capacitance is necessitated by the requirement for dc tracking. If the impedance of the network was not infinity at dc, constant tube deflections would require a ramp signal in charge (eventually saturating the amplifier), this is reflected in the scan filter  $F(s)$  and its inverse  $F(s)^{-1}$ .

To damp a single mode of structural vibration, the circuit inductance  $L$ , capacitance  $C$ , and piezoelectric capacitance  $C_p$  are tuned to resonate at the target mechanical frequency  $\omega_1$ . Although the capacitance value  $C$  is essentially arbitrary, values of 1 to 10 times the piezoelectric capacitance have been found suitable. To equate the frequency of electrical resonance to mechanical resonance, the inductor is tuned as follows:

$$L = \frac{C + C_p}{CC_p\omega_1}. \quad (22)$$

The resistance value, dependent on the inherent system damping, is most easily found experimentally. For such systems, resistances in the order of 1 k $\Omega$  are typical.

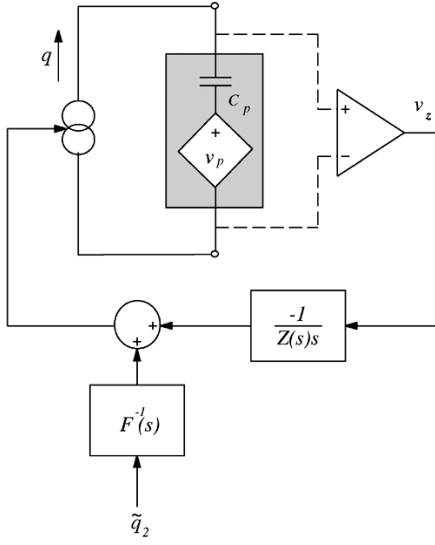


Fig. 12. Schematic diagram of a charge driven tube with integrated shunt circuit.

### III. IMPLEMENTATION

Resonant piezoelectric shunt damping circuits require impractically large values of inductance, typically in the tens of Henrys. For this reason the shunt damping circuit will be synthesized artificially using the charge amplifier. Consider the schematic shown in Fig. 12. Neglecting the filter  $F^{-1}(s)$  and input  $q_2$ , the charge applied to the piezoelectric tube is equal to

$$q = v_z \frac{-1}{sZ(s)}. \quad (23)$$

The impedance (or admittance) experienced by the piezoelectric transducer can be calculated by examining the ratio of current to voltage at its terminals. As the current is equal to  $-\dot{q}$ , and  $q$  is defined by (23), the impedance presented to the terminals is simply  $Z(s)$  (as defined by the filter in Fig. 12). By implementing the filter  $(-1/sZ(s))$  any arbitrary impedance can be presented to the terminals of the transducer. Simple techniques for designing analog and digital filters that represent  $(1/(Z(s)))$  can be found in [25]. In this work a dSpace DSP system is used to implement and tune the filter  $(-1/(sZ(s)))$ .

In addition to the charge required for shunt impedance synthesis, the additive charge  $q_2$  is used for tube scanning. As mentioned in Section II-B-1, the additive charge  $q_2$  requires a filter  $F^{-1}(s)$  to compensate for the electrical dynamics of the shunt impedance when attached to the same electrode.

A substantial simplification of the system shown in Fig. 12 can be made by studying the structure of the filter  $F^{-1}(s)$

$$\begin{aligned} F^{-1}(s) &= \frac{1}{K(s)Z(s)} = \frac{1 + C_p s Z(s)}{C_p s Z(s)} \\ &= \frac{1}{C_p s Z(s)} + 1. \end{aligned} \quad (24)$$

Considering that the transfer function  $(1/(sZ(s)))$  has already been implemented,  $F^{-1}(s)$  can be replaced as shown in Fig. 13.

#### A. DC Accurate Charge Amplifier

One of the key components utilized so-far without reference is the charge amplifier. As mentioned in the introduction, sub-

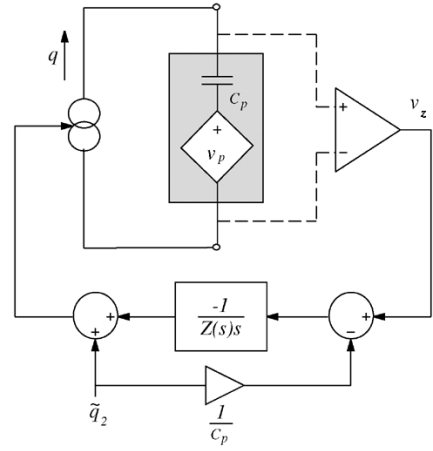


Fig. 13. Simplified diagram of a charge amplifier with integrated shunt impedance.

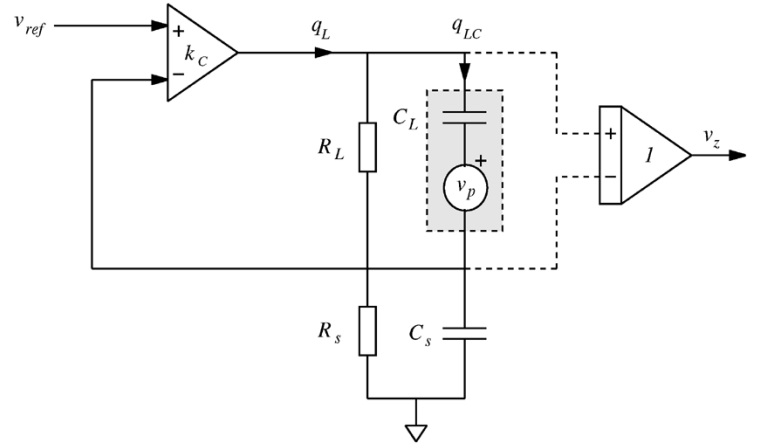


Fig. 14. Simplified diagram of a generic charge source.

stantial difficulties have been experienced in attempts to construct such a device for capacitive loads.

Consider the simplified diagram of a generic current source shown in Fig. 14. The piezoelectric load, modeled as a capacitor and voltage source  $v_p$ , is shown in gray. The high gain feedback loop ( $k_C$ ) works to equate the applied reference voltage  $v_{ref}$ , to the voltage across a sensing capacitor  $C_s$ . Neglecting the resistances  $R_L$  and  $R_s$ , at frequencies well within the bandwidth of the control loop, the load charge  $q_L$  is equal to

$$q_L = V_{ref} C_s \quad (25)$$

i.e., we have a charge amplifier with gain  $C_s$  Columbs/V.

The foremost difficulties associated with the charge amplifier shown in Fig. 14 are due to the resistances  $R_L$  and  $R_s$ . These resistances model the parasitic leakage resulting from the input terminals of the feedback opamps, capacitor dielectric leakage, and  $v_z$  measurement. In practice, this parasitic resistance is often swamped with additional physical resistances required to manage voltage drift associated with the input bias current of the opamps and voltage instrumentation.

If there exists a parallel load resistance  $R_L$ , the actual charge  $q_{LC}(s)$  flowing through the load transducer becomes

$$q_{LC}(s) = q_L(s) \frac{s}{s + \frac{1}{R_L C_L}}. \quad (26)$$

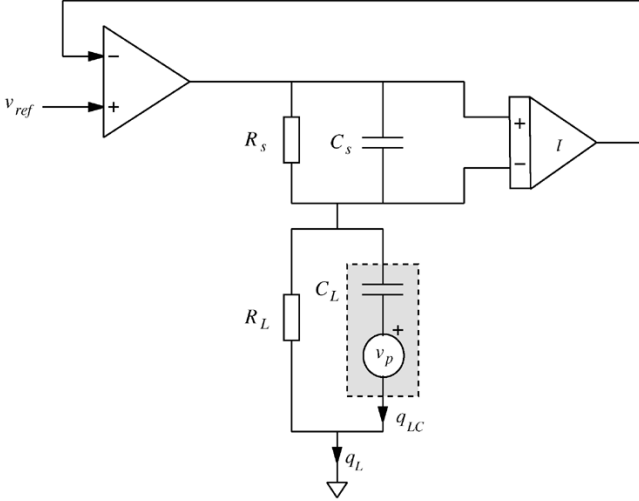


Fig. 15. DC accurate charge source for grounded capacitive loads.

The amplifier now contains a high-pass filter with cutoff  $\omega_c = (1/(R_L C_L))$ . That is

$$\frac{q_{LC}(s)}{V_{ref}(s)} = C_s \frac{s}{s + \frac{1}{R_L C_L}}. \quad (27)$$

In a typical piezoelectric tube drive scenario, with  $C_L = 10$  nF, a  $1 \mu$  A output offset current requires a 10-M $\Omega$  parallel resistance to limit the dc voltage offset to 10 V. Phase lead exceeds 5 degrees below 18 Hz. Such poor low-frequency performance precludes the use of charge amplifiers in applications requiring accurate low-frequency tracking, e.g., Atomic Force Microscopy [26].

A solution for the problem of voltage drift was first presented in [27]. An auxiliary voltage feedback loop was included to correct low-frequency behavior and allow for constant charge offsets. The circuit implementation required the design of separate voltage and charge feedback controllers. A simplified design relying on the intrinsic voltage control offered by the parasitic resistances was later presented in [28]. Neither of the amplifiers discussed have been capable of driving grounded loads. As piezoelectric tubes have multiple external electrodes and a common (often grounded) internal electrode, the requirement for a grounded-load is a necessity.

In the following, we present a dc accurate grounded-load charge amplifier. Shown in Fig. 15, the amplifier incorporates a high common-mode rejection, high common-mode range differential stage consisting of the lower opamp, voltage bridge, and instrumentation amplifier. The amplifier works to equate the voltage measured across the sensing impedance to the reference voltage  $v_{ref}$ .

To understand the operation of the amplifier we study the transfer function from the reference voltage  $v_{ref}$  to the load charge  $q_{LC}$ .

$$\frac{q_L(s)}{v_{ref}(s)} = C_s \frac{s + \frac{1}{C_s R_s}}{s} \quad (28)$$

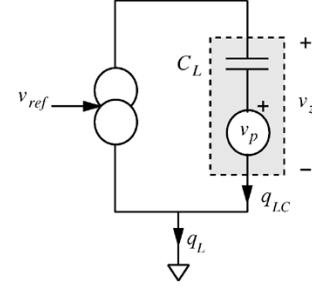


Fig. 16. Test for voltage/charge dominance.

The reference to actual load charge transfer function can be found by combining (28) and (26)

$$\begin{aligned} \frac{q_{LC}(s)}{v_{ref}(s)} &= \frac{q_L(s)}{v_{ref}(s)} \frac{q_{LC}(s)}{q_L(s)} \\ &= C_s \frac{s + \frac{1}{C_s R_s}}{s} \frac{s}{s + \frac{1}{R_L C_L}}. \end{aligned} \quad (29)$$

By setting  $C_L R_L = C_s R_s$ , i.e.

$$\frac{R_L}{R_s} = \frac{C_s}{C_L} \quad (30)$$

the amplifier has no low-frequency dynamics and constant gain  $C_s$  Columbs/V. Effectively the voltage amplifier, comprised of the two resistances  $R_L$  and  $R_s$ , synthesizes the operation of an ideal charge amplifier at low frequencies.

As the amplifier can be viewed as the concatenation of a voltage and charge amplifier, it is important to identify the frequency range where each mode of operation is dominant. Consider the schematic shown in Fig. 16. During perfect charge operation, i.e., when  $q_{LC}$  is correctly regulated to zero, the voltage  $v_z$  will be equal to  $v_p$ . During voltage dominant behavior,  $v_z$  will be regulated to zero. Such characteristics can easily be measured experimentally. Although the voltage dynamics have been designed to perfectly synthesize the operation of an ideal charge amplifier, during voltage dominant operation, if the load is not purely capacitive, errors in  $q_{LC}$  will occur.

When  $v_{ref} = 0$ , which implies  $q_L = 0$ , the transfer function from  $v_p$  to  $v_z$  reveals the voltage or charge dominance of the amplifier. At frequencies where  $v_z \approx v_p$ , the amplifier is charge dominant, and voltage dominant when  $v_z \approx 0$ . For the hybrid amplifier shown in Fig. 15, when  $v_{ref} = 0$

$$\frac{v_z(s)}{v_p(s)} = \frac{s}{s + \frac{1}{R_L C_L}} \quad (31)$$

i.e., at frequencies above  $(1/(R_L C_L)) s^{-1}$  the amplifier is charge dominant, and voltage dominant below. Obviously, given (31), the objective will be to select a load resistor  $R_L$  as large as possible. This may be limited by other factors such as opamp current noise attenuation, bias-current based offset voltages, and the common-mode and differential leakage of the opamp. In practice,  $(v_z(s))/(v_p(s))$  is best measured by simply applying a voltage to another electrode and using that as a reference, as the frequencies under consideration are well below the tube's first mechanical resonance, the applied voltage will be related by a constant.

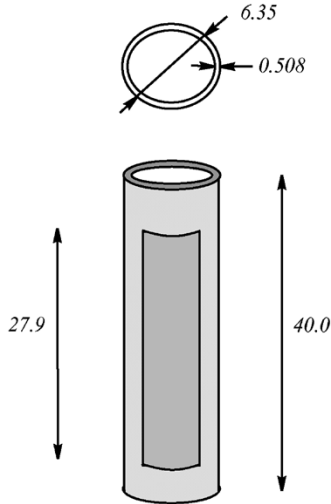


Fig. 17. Piezoelectric tube dimensions (in mm).

TABLE I  
PARAMETERS OF THE CHARGE AMPLIFIER AND SHUNT IMPEDANCE

Charge Gain	77.8 nC/V
Voltage Measurement Gain	0.1 V/V
$L$	2.9 H
$C$	50 nF
$R$	3.3 k $\Omega$

Alike a typical voltage amplifier, the hybrid amplifier offers little or no hysteresis reduction over the frequency range of voltage dominance. For the same reason, no improvement in creep can be expected. Creep time-constants are usually greater than 10 min, which in this discussion, is effectively dc. At these frequencies the amplifier behaves analogously to a standard voltage amplifier.

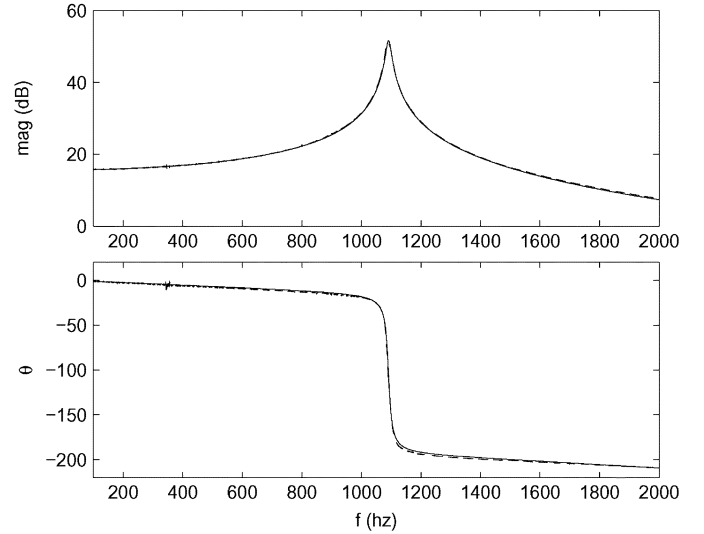
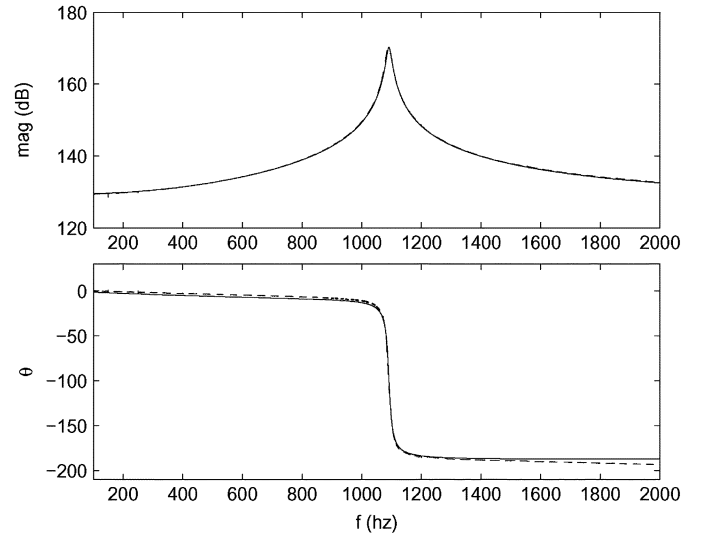
#### IV. EXPERIMENTAL RESULTS

In this section, the prototype shunt circuit and charge amplifier are employed to drive a piezoelectric tube positioner in one dimension. The tube was manufactured and patterned by Boston Piezo-Optics, physical dimensions can be found in Fig. 17. The tube was glued (with 24 h epoxy) vertically into a recessed (by 1.5 mm) aluminum block. An ADE Tech capacitive sensor was used to measure the displacement with sensitivity 10 V/ $\mu\text{m}$  and bandwidth 10 kHz. An aluminum cube (1 cm  $\times$  1 cm  $\times$  1 cm) is glued onto the tube tip and grounded to provide a return for the capacitive sensor. Both the tube block and sensor mount are affixed to a stabilized optical table. Parameters of the shunt impedance and amplifier are shown in Table I.

##### A. Tube Dynamics

We present the experimental results by first examining the natural response of the piezoelectric tube. The measured and identified transfer functions from charge input to strain-voltage and displacement are shown in Figs. 18 and 19. The system model  $G$  (shown in Fig. 6), was obtained by frequency domain subspace system identification [29]. The identification<sup>1</sup> required

<sup>1</sup>An implementation of the algorithm is freely available by contacting the author.

Fig. 18. The transfer function  $G_{dq}$  measured from the charge input  $q$  (C) to the measured displacement  $d$  (m). (—) Identified model, (- -) measured.Fig. 19. The transfer function  $G_{vq}$  measured from the charge input  $q$  (C) to the measured strain voltage  $v_p$  (V). (—) Identified model, (- -) measured.

12 MIMO data points to return a single input, two output model of order 2. An excellent fit is observed in the frequency domain.

The nominal first resonance frequency and dc charge sensitivity of the tube were measured to be 1088 Hz and 5.7 m/C (5.7  $\mu\text{m}/\mu\text{C}$ ).

##### B. Amplifier Performance

Both the low-frequency scanning and high-frequency vibration damping depend on the performance of the charge amplifier and related instrumentation. In the following we examine the two characteristics of foremost importance: low-frequency charge regulation—the ability of the amplifier to reproduce low-frequency inputs without drift, and the bandwidth of charge dominance—the frequency range where hysteresis will be reduced due to dominant charge feedback.

The (low-frequency) transfer function measured from an applied reference signal to the actual charge deposited on a 5-nF dummy load is shown in Fig. 20. Excellent low-frequency tracking from 15 mHz to 15 Hz is exhibited by the amplifier and

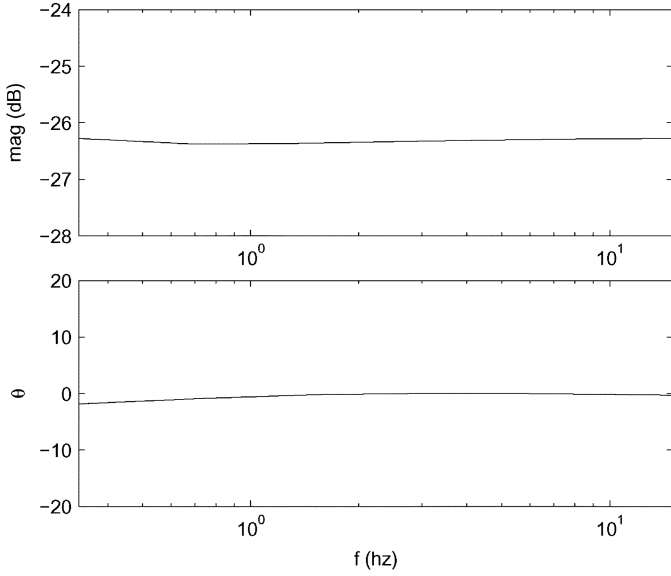


Fig. 20. Charge amplifier low-frequency tracking performance. Measured from the charge reference signal ( $V$ ) to the instrumented load voltage across a 5-nF dummy load.

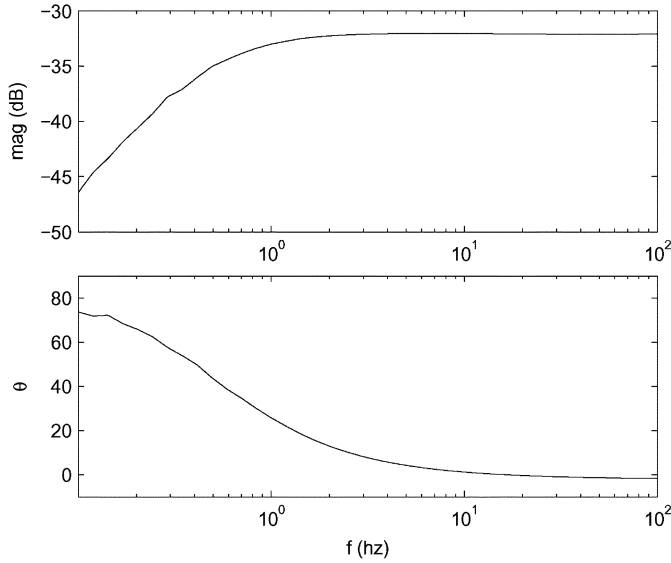


Fig. 21. Charge dominance bandwidth. Measured from the internal tube strain voltage  $v_p$  to the load voltage.

instrumentation. As discussed in Section III-A, the bandwidth of charge dominance was ascertained by zeroing the charge reference and introducing an internal load voltage. The transfer function measured from the internal voltage to the voltage measured across the load is shown in Fig. 21. We observe a charge dominance bandwidth of 0.8 Hz. Frequencies above this bandwidth will experience the full linearity benefit of charge actuation.

To justify the use of charge actuation we demonstrate the benefit in Figs. 22 and 23. Hysteresis is reduced by approximately 89% simply through the use of a charge amplifier. Percentage reduction is calculated by measuring the maximum excursion in the minor axis of each plot, then taking the ratio  $100 \times \frac{\text{voltage}}{\text{charge}}$ . It should be noted that a scan range of  $\pm 3 \mu\text{m}$  is around 20% of the

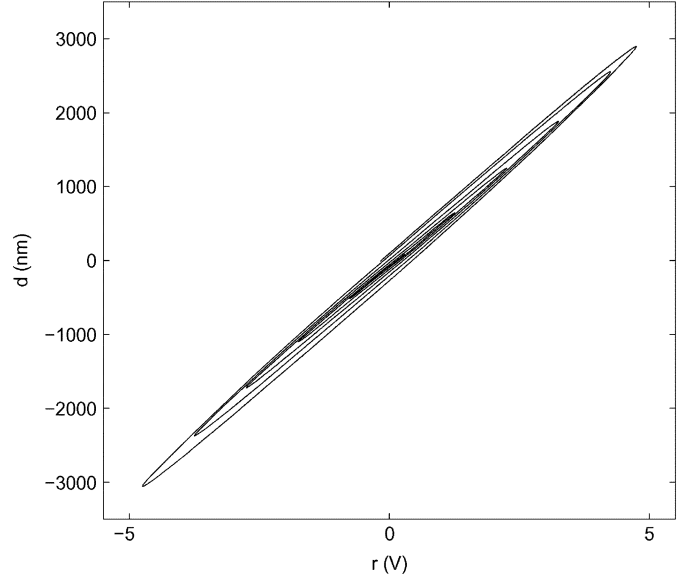


Fig. 22. Relationship between an applied voltage and the resulting tube displacement. (10-Hz ramped sinusoidal input.)

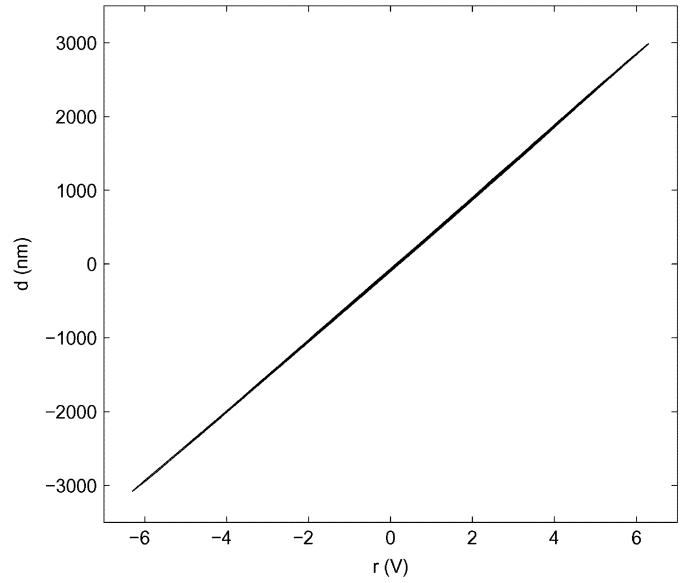


Fig. 23. Relationship between an applied charge reference and the resulting tube displacement. (10-Hz ramped sinusoidal input.)

full scale deflection, it is often assumed that hysteresis is negligible at such low drives. Similar plots for the same apparatus with a  $\pm 8 \mu\text{m}$  drive can be found in [27], a greater hysteresis is exhibited, and heavily reduced through the use of a similar charge drive.

### C. Shunt Damping Performance

1) *Scan Induced Vibration Suppression:* While scanning at high frequencies, the greatest cause of tracking error is due to high frequency harmonics exciting the mechanical resonance. The influence of the shunt impedance can be observed to significantly increase the effective damping in Fig. 24. The simulated response shown in Fig. 25 shows a good correlation with experimental results. The equivalent decrease in settling time can be observed in Fig. 26.

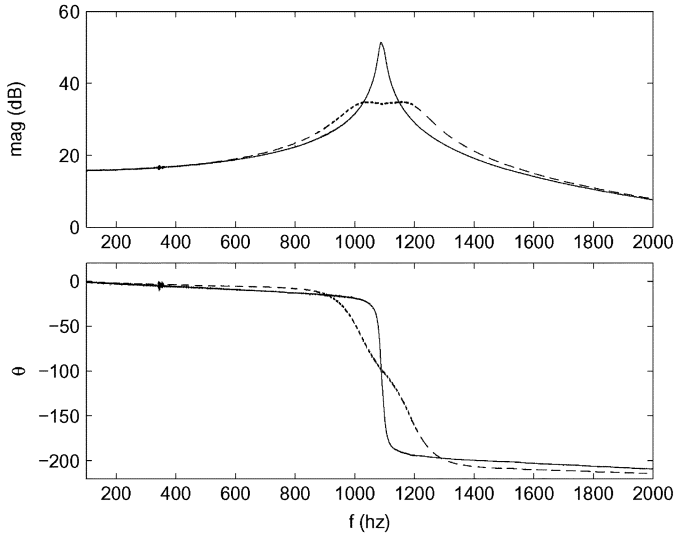


Fig. 24. Experimental response. Natural (—) and shunt-damped (- -) tube dynamics measured from the additive charge input  $q_2$  (C) to the tip displacement  $d$  (m).

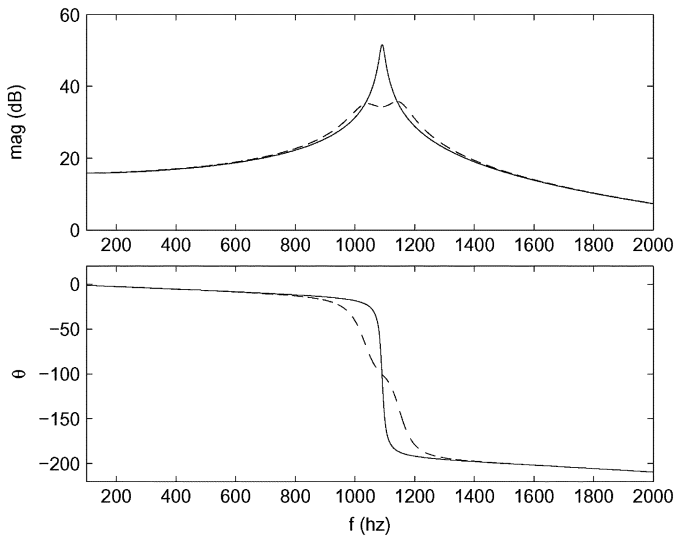


Fig. 25. Simulated response. Natural (—) and shunt-damped (- -) tube dynamics measured from the additive charge input  $q_2$  (C) to the tip displacement  $d$  (m).

The improvement in triangular scanning fidelity is illustrated in Fig. 27; an unfiltered 46-Hz Triangle wave was applied to the system. The frequency and lack of filtering was chosen to illustrate the worst-case induced ripple. In practice, the triangle would be filtered or passed through a feedforward controller to reduce vibration. Regardless of the ripple magnitude, the presence of a shunt circuit provides the same decrease in settling time. At high speeds, significant increases in fast-axis resolution can be expected. In the case where feedforward vibration control [11] is applied, the damped mechanical system would allow a less severe prefilter and provide greater immunity to modeling error.

2) *Externally Induced Vibration:* Another significant source of tracking error is external mechanical noise. Due to the highly resonant nature of the tube, high frequency noise components can excite the mechanical resonance and lead to large erroneous

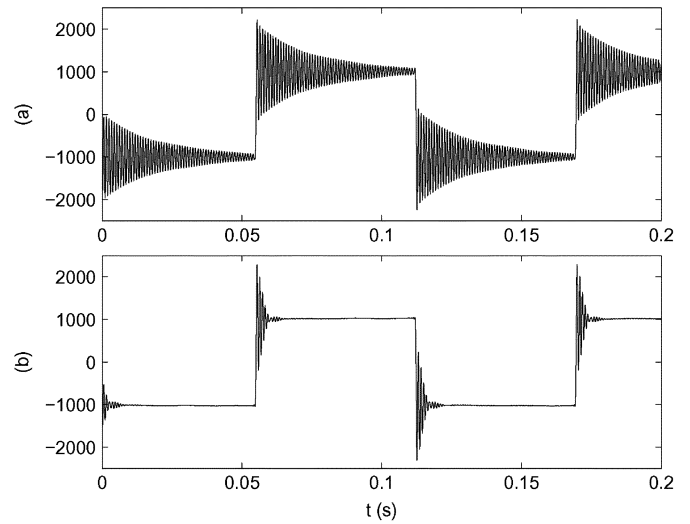


Fig. 26. Tube deflection (in nm) resulting from square wave excitation. (a) Uncontrolled and (b) with  $L - C - R$  shunt impedance.

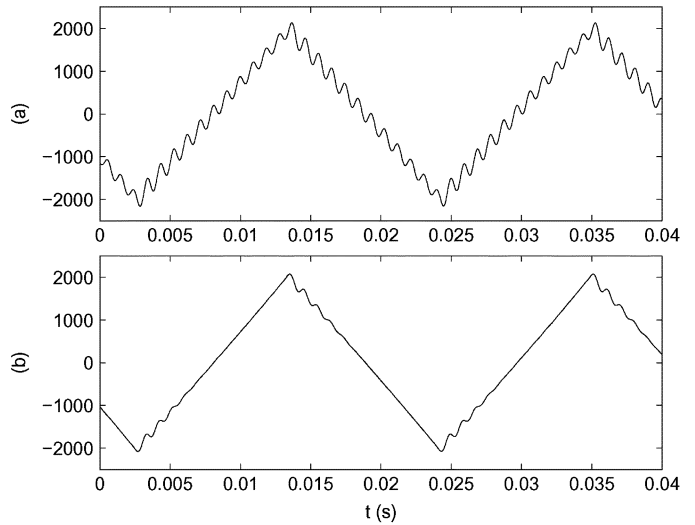


Fig. 27. Tube deflection (in nm) resulting from a 46-Hz triangle wave excitation. (a) Uncontrolled and (b) with  $L - C - R$  shunt impedance.

excursions. By applying a voltage to an opposite electrode, we can simulate the effect of a strain disturbance. A significant damping of greater than 20 dB can be observed in Fig. 28. The effect of such damping can be observed in the time domain by applying a low-frequency scanning signal. With no scan-induced vibration, the external noise is dominant. The reduction of resonant vibration can be seen in Fig. 29.

3) *Low-Frequency Scanning:* The final test of such an apparatus is the ability to track dc charge offsets. In Fig. 30 a low-frequency triangle signal was applied to the charge amplifier, at time 130 s, a dc offset equivalent to around  $1 \mu\text{m}$  was applied. Aside from the faithful reproduction of a 0.1-Hz triangle wave, the charge amplifier reproduces the offset without drift.

## V. CONCLUSION

In this paper, a new charge amplifier has been presented for the reduction of hysteresis in piezoelectric tube scanners. Using the intrinsic voltage feedback offered by parasitic resistances,

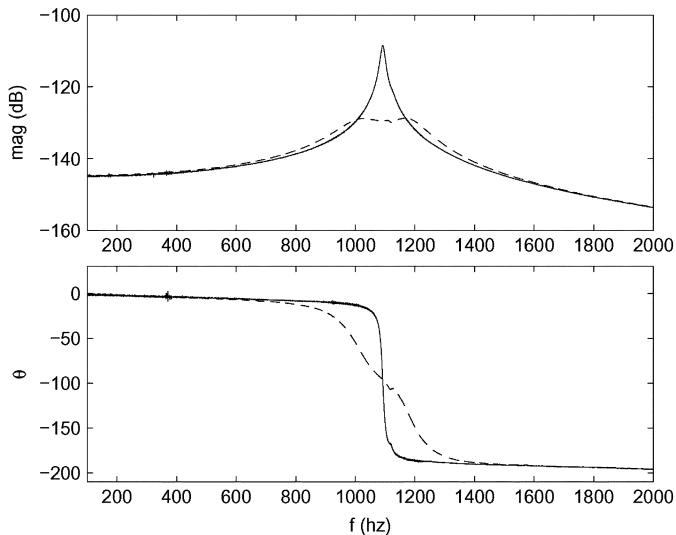


Fig. 28. Experimental response. The natural (—) and shunt-damped (- -) tube transfer function from the applied strain disturbance (in  $V$ ) to the tip displacement  $d$  ( $m$ ).

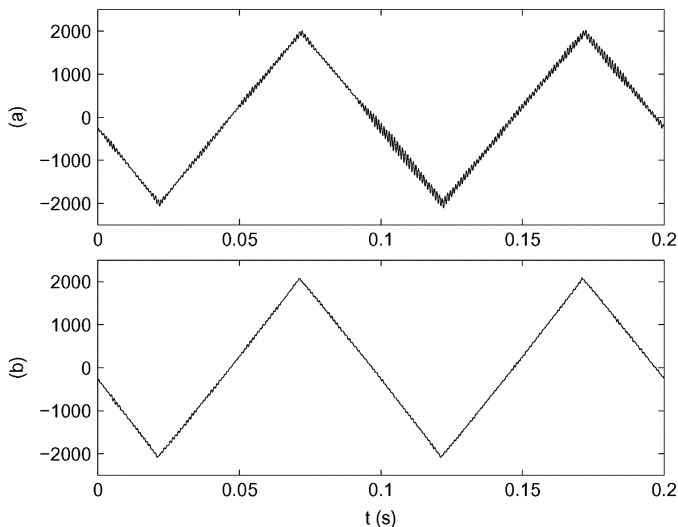


Fig. 29. Tube deflection (in  $nm$ ) resulting from a 1.6-kHz band-limited uniformly distributed random strain disturbance. (a) Uncontrolled and (b) with  $L - C - R$  shunt impedance.

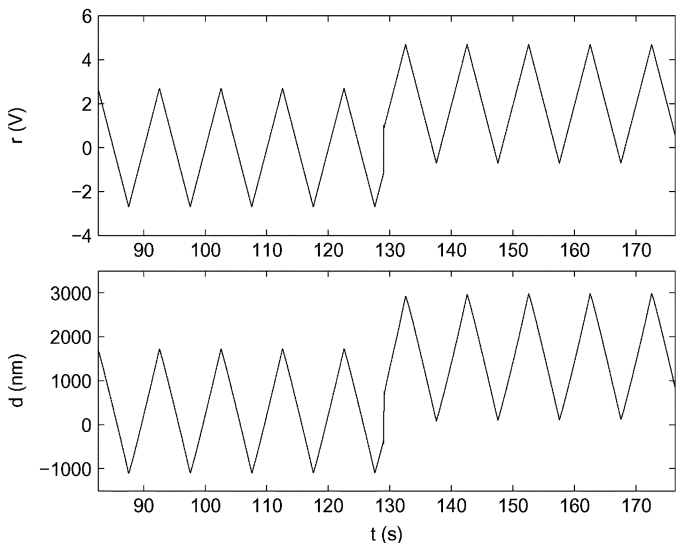


Fig. 30. Low-frequency scanning reference and resultant tube displacement with additive dc offset.

low-frequency voltage drift has been eliminated to provide dc accurate operation. The proposed charge amplifier is simple to fabricate and easily integrated into existing open-loop or controlled systems.

In addition to hysteresis reduction, piezoelectric shunt damping has been applied to reduce scan-induced vibration. Piezoelectric shunt damping involves the connection of an electrical impedance to the terminals of a piezoelectric transducer. In experiments considering scan-induced and externally induced vibration, an LCR network reduces the first resonance frequency by 20 dB in magnitude. No feedback sensors are required.

Although charge-driven shunt-damped piezoelectric tubes can be integrated into previous design methodologies, the simplicity of implementation and performance warrants their use independently. Current work includes the design of an all-analog amplifier incorporating both charge actuation, and shunt impedance implementation.

## REFERENCES

- [1] G. Binnig and D. P. E. Smith, "Single-tube three-dimensional scanner for scanning tunneling microscopy," *Rev. Sci. Instrum.*, vol. 57, no. 8, pp. 1688–1689, Aug. 1986.
- [2] E. Meyer, H. J. Hug, and R. Bennewitz, *Scanning Probe Microscopy*. Heidelberg, Germany: Springer, 2004.
- [3] D. Croft, D. McAllister, and S. Devasia, "High-speed scanning of piezo-probes for nano-fabrication," *Trans. ASME, J. Manufact. Sci. Technol.*, vol. 120, pp. 617–622, Aug. 1998.
- [4] W. Gao, R. J. Hocken, J. A. Patten, J. Lovingood, and D. A. Lucca, "Construction and testing of a nanomachining instrument," *Precision Eng.*, vol. 24, no. 4, pp. 320–328, Oct. 2000.
- [5] *IEEE Standard on Piezoelectricity*, 1988. I. of Electrical and E. E. Inc., ANSI/IEEE Std. 176-1987.
- [6] C. J. Chen, "Electromechanical deflections of piezoelectric tubes with quartered electrodes," *Appl. Phys. Lett.*, vol. 60, no. 1, pp. 132–134, Jan. 1992.
- [7] H. J. M. T. A. Adriaens, W. L. de Koning, and R. Banning, "Modeling piezoelectric actuators," *IEEE/ASME Trans. Mechatron.*, vol. 5, no. 4, pp. 331–341, Dec. 2000.
- [8] D. Croft, S. Stilson, and S. Devasia, "Optimal tracking of piezo-based nanopositioners," *Nanotechnology*, vol. 10, pp. 201–208, 1999.
- [9] K. Leang and S. Devasia, "Iterative feedforward compensation of hysteresis in piezo positioners," in *IEEE Conf. Decision Control*, Maui, HI, Dec. 2003.
- [10] G. Schitter, R. W. Stark, and A. Stemmer, "Fast contact-mode atomic force microscopy on biological specimens by model-based control," *Ultramicroscopy*, vol. 100, pp. 253–257, 2004.
- [11] D. Croft, G. Shed, and S. Devasia, "Creep hysteresis, and vibration compensation for piezoactuators: Atomic force microscopy application," *Trans. ASME, J. Dynam. Syst., Meas. Control*, vol. 123, pp. 35–43, Mar. 2001.
- [12] K. J. G. Hinnen, R. Fraanje, and M. Verhaegen, "The application of initial state correction in iterative learning control and the experimental validation on a piezoelectric tube scanner," *J. Syst. Contr. Eng.*, vol. 218, pp. 503–511, 2004.
- [13] G. Schitter and A. Stemmer, "Model-based signal conditioning for high-speed atomic force and friction force microscopy," *Microelectron. Eng.*, vol. 67–68, pp. 938–944, 2003.
- [14] H. Perez, Q. Zou, and S. Devasia, "Design and control of optimal scan trajectories: Scanning tunneling microscope example," *J. Dynam. Syst., Meas. Control*, vol. 126, pp. 187–197, Mar. 2004.
- [15] S. Salapaka, A. Sebastian, J. P. Cleveland, and M. V. Salapaka, "High bandwidth nano-positioner: A robust control approach," *Rev. Sci. Instrum.*, vol. 75, no. 9, pp. 3232–3241, Sep. 2002.
- [16] C. V. Newcomb and I. Flinn, "Improving the linearity of piezoelectric ceramic actuators," *Inst. Elect. Eng. Electron. Lett.*, vol. 18, no. 11, pp. 442–443, May 1982.
- [17] P. Ge and M. Jouaneh, "Tracking control of a piezoelectric actuator," *IEEE Trans. Contr. Syst. Technol.*, vol. 4, no. 3, pp. 209–216, May 1996.

- [18] J. M. Cruz-Hernandez and V. Hayward, "Phase control approach to hysteresis reduction," *IEEE Trans. Contr. Syst. Technol.*, vol. 9, no. 1, pp. 17–26, Jan. 2001.
- [19] H. Kaizuka and B. Siu, "Simple way to reduce hysteresis and creep when using piezoelectric actuators," *Japan J. Appl. Phys., Part 2—Lett.*, vol. 27, no. 5, pp. 773–776, May 1988.
- [20] R. L. Forward, "Electronic damping of vibrations in optical structures," *Appl. Opt.*, vol. 18, no. 5, pp. 690–697, Mar. 1979.
- [21] N. W. Hagood and A. Von Flotow, "Damping of structural vibrations with piezoelectric materials and passive electrical networks," *J. Sound Vib.*, vol. 146, no. 2, pp. 243–268, 1991.
- [22] S. O. R. Moheimani, A. J. Fleming, and S. Behrens, "On the feedback structure of wideband piezoelectric shunt damping systems," *IOP Smart Materials and Structures*, vol. 12, pp. 49–56, Jan. 2003.
- [23] A. J. Fleming, "Synthesis and implementation of sensor-less shunt controllers for piezoelectric and electromagnetic vibration control," Ph.D. dissertation, The University of Newcastle, Australia, Feb. 2004.
- [24] S. O. R. Moheimani, "A survey of recent innovations in vibration damping and control using shunted piezoelectric transducers," *IEEE Trans. Contr. Syst. Technol.*, vol. 11, no. 4, pp. 482–494, Jul. 2003.
- [25] A. J. Fleming and S. O. R. Moheimani, "Improved current and charge amplifiers for driving piezoelectric loads, and issues in signal processing design for synthesis of shunt damping circuits," *Intell. Mater. Syst. Structures*, vol. 15, no. 2, pp. 77–92, Feb. 2004.
- [26] D. Croft, G. Shedd, and S. Devasia, "Creep, hysteresis and vibration compensation for piezoactuators: Atomic force microscopy application," in *Proc. American Control Conf.*, Chicago, IL, Jun. 2000, pp. 2123–2128.
- [27] A. J. Fleming and S. O. R. Moheimani, "Hybrid DC accurate charge amplifier for linear piezoelectric positioning," in *Proc. 3rd IFAC Symp. Mechatron. Syst.*, Sydney, NSW, Australia, Sep. 2004.
- [28] K. A. Yi and R. J. Veillette, "A charge controller for linear operation of a piezoelectric stack actuator," *IEEE Trans. Contr. Syst. Technol.*, vol. 13, no. 4, pp. 517–526, Jul. 2005.
- [29] T. McKelvey, H. Akcay, and L. Ljung, "Subspace based multivariable system identification from frequency response data," *IEEE Trans. Autom. Control*, vol. 41, no. 7, pp. 960–978, Jul. 1996.



**Andrew J. Fleming** (M'01) was born in Dingwall, Scotland, in 1977. He received the B.E. degree in electrical engineering from The University of Newcastle, Australia, in 2000 and the Ph.D. degree in 2004.

He is a Research Academic with the Centre for Complex Dynamic Systems and Control, an Australian Government Special Research Centre. His research includes nanopositioning and sensor-less control of sound and vibration.



**S. O. Reza Moheimani** (S'93–M'97–SM'00) received the B.Sc. degree from Shiraz University in 1990 and the M.Eng.Sc. and Ph.D. degrees from the University of New South Wales, Australia, in 1993 and 1996, respectively, all in electrical and electronics engineering.

In 1996, he was a Postdoctoral Research Fellow with the School of Electrical and Electronics Engineering, Australian Defence Force Academy, Canberra, Australia. In 1997, he joined the University of Newcastle, Australia, where he is currently an Associate Professor with the School of Electrical Engineering and Computer Science.

His research interests include smart structures, mechatronic systems, control theory, and signal processing. He has more than 100 journal and conference publications, is a coauthor of the research monograph *Spatial Control of Vibration: Theory and Experiments* (Singapore: World Scientific, 2003) and the editor of the volume *Perspectives in Robust Control* (New York: Springer-Verlag, 2001).

Dr. Moheimani is an Associate Editor of *IEEE TRANSACTIONS ON CONTROL SYSTEMS TECHNOLOGY*, and the *International Journal of Control, Automation, and Systems* and a past Associate Editor of *Control Engineering Practice*. He has served on the editorial boards of several international conferences, and was the Chairman of International Program Committee for the 3rd IFAC Symposium on Mechatronic Systems, held in Sydney, Australia, in September 2004. He is a member of the ARC Centre for Complex Dynamic Systems and Control, where he directs the Centre's research in the area of mechatronics.